

Evidence of Magnon-Mediated Orbital Magnetism in a Quasi-2D Topological Magnon Insulator

Laith Alahmed,¹ Xiaoqian Zhang,² Jiajia Wen,³ Yuzan Xiong,⁴ Yi Li,⁵ Li-chuan Zhang,⁶ Fabian Lux,⁷ Frank Freimuth,^{6,7} Muntasir Mahdi,¹ Yuriy Mokrousov,^{6,7} Valentine Novosad,⁵ Wai-Kwong Kwok,⁵ Dapeng Yu,² Wei Zhang,⁴ Young S. Lee,^{3,8} and Peng Li¹

¹*Department of Electrical and Computer Engineering, Auburn University, Auburn, AL 36849, USA*

²*Shenzhen Institute for Quantum Science and Engineering, Southern University of Science and Technology, Shenzhen, 518055, China*

³*Stanford Institute for Materials and Energy Sciences, SLAC National Accelerator Laboratory, Menlo Park, CA, 94025, USA*

⁴*Department of Physics, Oakland University, Rochester, MI 48309 USA*

⁵*Materials Science Division, Argonne National Laboratory, Lemont, IL 60439*

⁶*Peter Grünberg Institut and Institute for Advanced Simulation, Forschungszentrum Jülich and JARA, 52425 Jülich, Germany*

⁷*Institute of Physics, Johannes Gutenberg University Mainz, 55099 Mainz, Germany*

⁸*Department of Applied Physics, Stanford University, Stanford, CA, 94305, USA*

ABSTRACT: We explore spin dynamics in Cu(1,3-bdc), a quasi-2D topological magnon insulator. The results show that the thermal evolution of Landé g -factor (g) is anisotropic: $g_{\text{in-plane}}$ reduces while $g_{\text{out-plane}}$ increases with increasing temperature T . Moreover, the anisotropy of the g -factor (Δg) and the anisotropy of saturation magnetization (ΔM_s) are correlated below 4 K, but they diverge above 4 K. We show that the electronic orbital moment contributes to the g anisotropy at lower T , while the topological orbital moment induced by thermally excited spin chirality dictates the g anisotropy at higher T . Our work suggests an interplay among topology, spin chirality, and orbital magnetism in Cu(1,3-bdc).

KEYWORDS: topological orbit moment, topological magnon insulator, Kagome magnet, magnon excitation, g -factor anisotropy

The discovery of topologically protected states in some systems with fermionic particles (e.g. electrons and holes) led to extensive research on topological insulators unraveling their unique properties[1]. Such topology-protected states can also exist within the band gap of systems with bosonic quasi-particles, such as photons [2, 3], phonons [4] and magnons [5–10], which can mediate the transport of spin and orbital angular momentum [11–14]. While the interplay between the topology of electronic bands and spin transport properties has been intensively studied [15–17], the relationship between magnonic topology and intrinsic magnetic properties remains largely unexplored [7].

Non-trivial magnonic band topology was predicted in magnonic crystals such as $\text{Lu}_2\text{V}_2\text{O}_7$ and $\text{Cu}[1,3\text{-benzenedicarboxylate}(\text{bdc})]$ [5]. $\text{Cu}(1,3\text{-bdc})$ is a metal-organic hybrid material where Cu^{2+} ions are arranged in a geometrically perfect Kagome lattice structure. The organic (1,3-bdc) molecules separate the individual Kagome planes, leading to weak interlayer interaction. It is thus identified as the first quasi-two-dimensional (2D) topological magnon insulator where strong exchange coupling is confined within individual layers [18]. Recent neutron scattering experiments identified flat bands originating from the unique geometry of the Kagome lattice, which can be described by a Heisenberg Hamiltonian with Dzyaloshinskii-Moriya interaction [19, 20]. Thus, these exotic properties make $\text{Cu}(1,3\text{-bdc})$ an ideal material platform for exploring the interplay

between magnonic topology and intrinsic magnetic properties including magnetization dynamics [21].

A recent theory proposed that chiral magnetism and topological magnonic excitations can be correlated with electronic orbital magnetism [22, 23]. In particular, it is suggested that orbital magnetization can play a significant role in the dynamics of collinear antiferromagnets with weak spin-orbit coupling [22]. However, experimental evidence concerning the role of magnon-mediated electronic orbital moment in magnetization dynamics is still lacking. In this regard, it is crucial to carry out experiments to uncover the underlying physics on this topic.

Here, we use $\text{Cu}(1,3\text{-bdc})$ as a model material to study the correlation of Landé g -factor and orbital angular momentum through Vibrating Sample Magnetometry (VSM), Superconducting Quantum Interference Device (SQUID), and broadband Ferromagnetic Resonance (FMR) spectroscopy. The experimental results show an anisotropic gyromagnetic ratio and a corresponding g -factor tensor. This anisotropy is found to be correlated with the difference in In-Plane (IP) and Out-Of-Plane (OOP) saturation magnetization at lower temperatures ($T < 4$ K); it indicates a contribution from electronic orbital moment. Surprisingly, such correlation breaks down when $T > 4$ K. Further analysis reveals that magnon-mediated electronic topological orbital moment has contributed to the magnetic moment at higher temperatures. We have built a foundation for elucidating

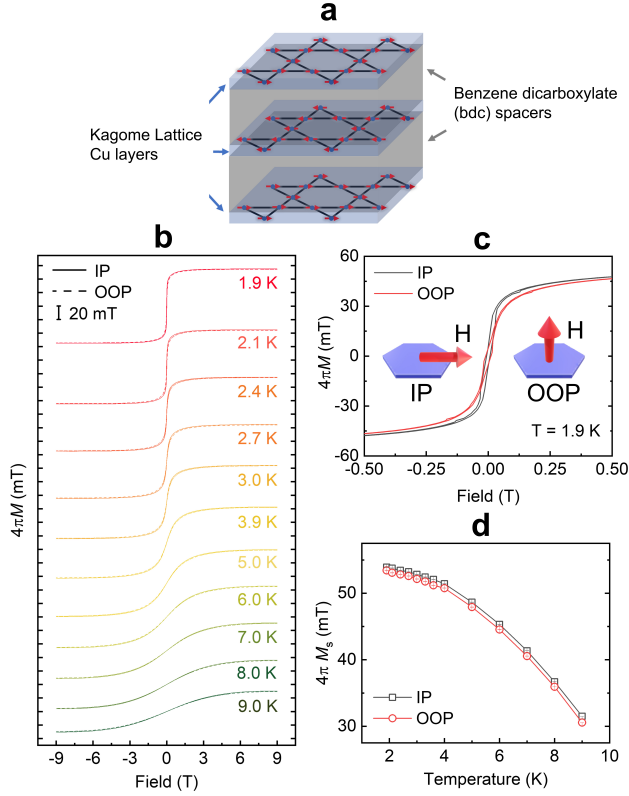


FIG. 1. Quasi-static magnetic properties of Cu(1,3-bdc). **a.** Schematic of Cu(1,3-bdc) structure. Kagome lattice Cu layers are spaced by Benzene dicarboxylate (bdc) organic layers. Red arrows represent spins within the Kagome lattice. **b.** Magnetization vs. externally applied field plots at different temperatures. The magnetic field was applied along the Kagome plane (IP) of the Cu(1,3-bdc) sample (solid lines), and perpendicular (OOP) to the Kagome plane (dashed lines). **c.** Zoomed-in IP and OOP hysteresis loops at $T = 1.9$ K, showing IP anisotropy. The left and right insets show the IP and OOP field directions, respectively. **d.** Temperature dependence of $M_{s,IP}$ (gray) and $M_{s,OOP}$ (red) extracted from the VSM measurements.

the intriguing interplay of topology, spin excitations, and electronic orbital magnetism. This work also highlights the unique properties of quasi-2D topological magnon insulators for building novel spintronic devices.

It was previously shown that, in the ground state of Cu(1,3-bdc), spins within each Kagome plane are ferromagnetically ordered, while spins in neighboring planes are antiferromagnetically ordered (Fig. 1a). The interlayer antiferromagnetic coupling was found to be $\sim 0.3\%$ of the intralayer nearest-neighbor coupling. Thus, the magnetization across different Kagome planes can be easily aligned by a weak magnetic field (\sim tens of mT)[20].

The quasi-static magnetization data of Cu(1,3-bdc) are presented in Fig. 1. Here, several notes should be

made: First, the magnetization as a function of IP and OOP fields at temperatures ranging from 1.9 K to 9 K was measured (Fig. 1a). Consistent with the previous measurement[20], Cu(1,3-bdc) favors a slight in-plane alignment. Second, Cu(1,3-bdc) is a quasi-2D material. It is estimated that the inter-Kagome-plane interaction is about 0.3% of the intra-Kagome-plane interaction. The three-dimensional Néel transition at ~ 1.8 K corresponds to the antiferromagnetic ordering of the spins on different Kagome planes, which is driven by the weak inter-plane interaction. The dominant intra-Kagome-plane interaction, which is ferromagnetic, is responsible for the short-range ferromagnetic ordering within each plane that persists well above the transition temperature of 1.8 K[20]. Thus, we summarize the magnetic transitions in Cu(1,3-bdc) as follows: when $T < 1.8$ K, Cu(1,3-bdc) exhibits antiferromagnetic ordering of the spins on different Kagome planes. When $1.8 \text{ K} < T < 9$ K, short-range ferromagnetic ordering exists within each plane. When $T > 9$ K, it transitions into a more paramagnetic state. Third, the magnetization curves were fitted with a hyperbolic tangent function to extract the saturation magnetization M_s [24] (refer to Supplementary Note V for details). The temperature dependence of the IP and OOP saturation magnetization $M_{s,IP}$, $M_{s,OOP}$ is plotted in Fig. 1c. Intriguingly, $M_{s,IP}$ is higher than that of $M_{s,OOP}$ across all tested temperatures (1.9 K to 9 K). For example, $M_{s,IP}$ is $\sim 0.8\%$ larger than $M_{s,OOP}$ at 1.9 K, which has been confirmed by both the VSM and SQUID measurements. This effect is also observed in the previous magnetization measurement[20]. With the hypothesis that the difference in $M_{s,IP}$ and $M_{s,OOP}$ resulted from orbital magnetic moment[22, 23], we carry out magnetization dynamics measurements to verify this understanding.

Fig. 2 presents the FMR data. A schematic of the FMR measurement is shown in Fig. 2a. A microwave diode and lock-in amplifier were used for signal detection. A Vector Network Analyzer (VNA) was also used to perform the FMR measurements and generated consistent data (See Supplementary Note 7 for details). Figs. 2b,c show microwave power absorption vs. external field at microwave frequencies ranging from 3 GHz to 27 GHz at 1.9 K along the IP and OOP directions, respectively. The FMR profiles were measured at temperatures up to 10 K. At each microwave frequency f , the FMR profiles were fitted to Lorentzian + anti-Lorentzian functions[25, 26] to extract the resonance field H_r , and the Full Width at Half Maximum (FWHM) linewidth ΔH_{FWHM} (See Supplementary Note 8). The resonance frequencies are plotted against the fitted IP and OOP resonance fields as shown in Figs. 2d,e. We adopt $H_r - H_{offset}$ as the horizontal axes, where $H_{offset} = 0.4$ T. These plots reveal a linear relationship between the resonance frequency and the resonance magnetic field (refer to Supplementary Note VI for details). The data

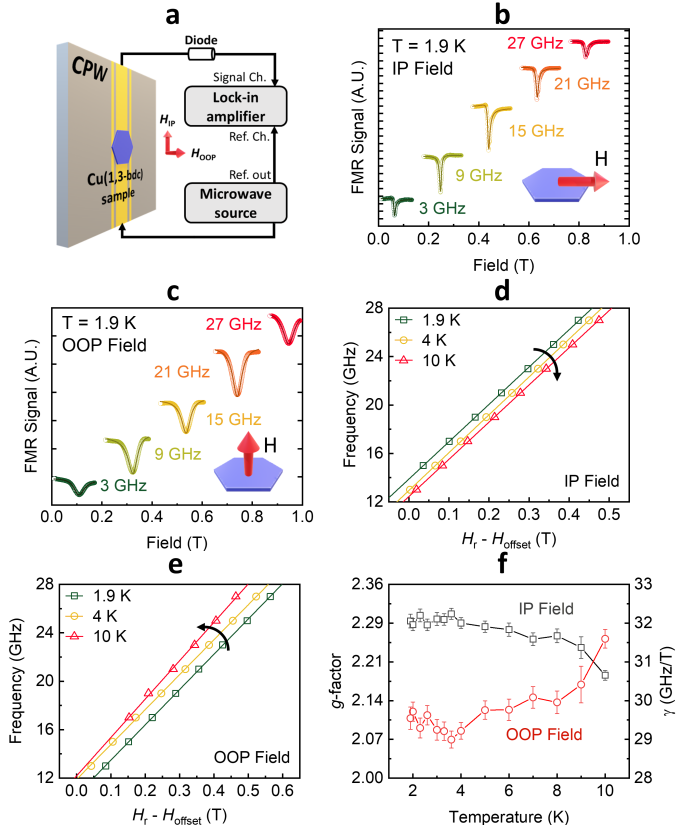


FIG. 2. Broadband FMR spectroscopy and analysis. **a.** Schematic of the experimental setup. **b.** and **c.** FMR profiles measured at different microwave frequencies at $T = 1.9$ K for IP and OOP fields, respectively. Both the datapoints and fitted curves are presented. The insets in **b** and **c** show the IP and OOP field directions, respectively. **d.** and **e.** Resonance frequency f vs. resonance field $H_r - H_{\text{offset}}$ at 1.9 K, 4 K, and 10 K for external fields applied IP and OOP, respectively. Here, $H_{\text{offset}} = 0.4$ T. The datapoints are fitted to Kittel Equations 1 and 2, respectively. The arrows denote the behavior of increasing temperature. **f.** Temperature dependence of the Landé g -factor (left axis) and gyromagnetic ratio γ (right axis) for external fields along the IP (gray) and OOP (red) directions.

points can be fitted by the Kittel equations[26]:

$$f = \gamma'_{\text{IP}} \sqrt{(H_r + 4\pi M_{\text{eff}})H_r} \quad (1)$$

$$f = \gamma'_{\text{OOP}} (H_r - 4\pi H_{\text{eff}}) \quad (2)$$

Equations (1) and (2) are for the IP and OOP cases, respectively. Here, f is the microwave frequency, $\gamma' = \frac{\gamma}{2\pi}$ is the reduced gyromagnetic ratio, and H_{eff} is the effective field representing the contribution from magnetocrystalline anisotropy. The g -factor is calculated using $g = |\gamma| \frac{\hbar}{\mu_B}$, where μ_B is the Bohr magneton and \hbar is the reduced Planck constant.

Fig. 2f plots the temperature dependence of the g -factor (left Y-axis) and γ' (right Y-axis) along the IP

and OOP fields, respectively. Several observations can be made from Fig. 2f: First, in both IP and OOP cases, the g -factor deviates from $g = 2$ that is for a free electron without orbital momentum. This deviation indicates an orbital contribution to the magnetic moment in Cu(1,3-bdc)[27, 28]. Second, g_{IP} is significantly larger than g_{OOP} at lower temperatures (i.e., < 9 K). Third, the thermal evolution of g_{IP} and g_{OOP} shows opposite trends: g_{IP} reduces with increasing temperature, while g_{OOP} increases with increasing temperature.

Both the quasi-static and dynamic magnetization measurements suggest the footprint of electronic orbital moment. Thus, the difference of the g -factor $\Delta g = g_{\text{IP}} - g_{\text{OOP}}$ is plotted together with the difference of the saturation magnetization $\Delta M_s = M_{s,\text{IP}} - M_{s,\text{OOP}}$ in Fig. 3a. Fig. 3a shows two contrasting behaviors, a low-temperature regime where the behavior of Δg is similar to ΔM_s with no significant deviation at $T < 4$ K, and a high-temperature regime where Δg deviates greatly from ΔM_s at $T > 4$ K.

It is thus insightful to interpret the temperature-dependent anisotropy of the g -factor in terms of the dynamics of orbital magnetism. At low temperatures, the g -factor anisotropy can be attributed to the anisotropy of the orbital magnetization in Cu(1,3-bdc) along the IP and OOP directions, with the IP case having a greater orbital contribution. The deviation of Δg from ΔM_s at higher temperatures comes as a surprise, because they are expected to be closely correlated at all temperatures. Thus, this points to a different mechanism to the orbital correction of the g -factor; it cannot be explained by the orbital motion of electrons around atomic cores.

A recent theoretical work uncovered contributions to electronic orbital magnetism originating from spin chirality generated from spin disorder[13, 29]. This new development in the area of thermally-driven spin fluctuations points out a route to explain the observed behavior in Cu(1,3-bdc). According to the theory, the non-vanishing net spin chirality can arise even in a collinear fluctuating spin system in its ground state. This can be directly translated into a topological electronic orbital motion, the strength of which is given by the topological orbital susceptibility relating the degree of the chirality to the magnitude of the orbital magnetization [30]. The magnitude of the topological orbital susceptibility can be sizable in materials with weak spin-orbit coupling, i.e. Cu(1,3-bdc), as shown in conventional microscopic calculations. Furthermore, in ferromagnetic Kagome systems with non-trivial topological magnonic bands, the spin chirality mediated by thermal fluctuations can imprint sizeable electronic orbital magnetization; their sign and magnitude are controlled by the parameters of the studied system [13].

Following the approach in Ref. [13], we use the extracted parameters which describe the spin-exchange interactions in Cu(1,3-bdc) [19] to compute the magnonic

properties. The calculation yielded thermally induced net chirality and corresponding orbital magnetization in the system. Specifically, we use the effective spin Hamiltonian of Cu(1,3-bdc) in Eq.(3):

$$H = -\frac{1}{2} \sum_{ij} J_{ij} \mathbf{S}_i \cdot \mathbf{S}_j - \frac{1}{2} \sum_{ij} \mathbf{D}_{ij} \cdot (\mathbf{S}_i \times \mathbf{S}_j) - \mathbf{B} \cdot \kappa^{\text{TO}} \sum_{ijk} \hat{\mathbf{e}}_{ijk} [\hat{\mathbf{S}}_i \cdot (\hat{\mathbf{S}}_j \times \hat{\mathbf{S}}_k)] - \mu_B g_e \mathbf{B} \cdot \sum_i \mathbf{S}_i, \quad (3)$$

where J_{ij} mediates the Heisenberg exchange between spins \mathbf{S}_i and \mathbf{S}_j on sites i and j in the first term. The second term is the antisymmetric Dzyaloshinskii-Moriya Interaction (DMI) quantified by vectors \mathbf{D}_{ij} . The fourth term couples the spins to an external magnetic field \mathbf{B} . The third term is the ring-exchange interaction term, which explicitly describes the Zeeman interaction of the topological orbital moment (TOM, \mathbf{L}^{TOM}) with the external magnetic field \mathbf{B} [13]. TOM marks a special type of electronic orbital moment. This term is given by the product of the scalar spin chirality (SSC) and the topological orbital susceptibility κ^{TO} [29–32]. Owing to the symmetry of the planar Kagome lattice, both the TOM and DMI vectors are perpendicular to the Kagome plane (OOP), in the same direction as the applied external magnetic field \mathbf{B} . In Eq.(3), the spin operator \mathbf{S}_i at site i is set as $\frac{1}{2}$, g_e is set as 2, the nearest-neighbor exchange interaction J is chosen as 0.6 meV and the DMI vector is set as $\mathbf{D}_{ij} = (0, 0, 0.09)$ meV. The topological orbital susceptibility κ^{TO} is chosen as a typical value of $-0.2\mu_B$, as suggested by the previous studies [29–32].

In Fig. 3b, we plot the magnonic band-resolved contributions to the orbital moment in Cu(1,3-bdc) for $B = 0$. One can see a strong correlation between the orbital moment and the topological band inversion of magnonic bands at low energies and between the first and second modes. Then, we integrate the contribution of the band-resolved orbital moment to the overall orbital moment of Cu(1,3-bdc) at finite temperatures. Fig. 3c presents the calculated TOM as a function of temperature and polar angle θ that indicates the magnetization direction. From Fig. 3c, two observations are made: First, the analysis shows that the symmetry of the system allows orbital magnetization originating from spin excitations in the OOP case but prohibits it in the IP case. Second, the value of the thermally-induced orbital moment increases monotonously with temperature and becomes sizable when $T > 4$ K along the OOP direction. In Fig. 3d, the differences of the g -factor ($\Delta g' = g_{\text{OOP}} - g_{\text{IP}}$) and ($\Delta \text{TOM} = \text{TOM}_{\text{OOP}} - \text{TOM}_{\text{IP}}$) are plotted as a function of temperature. One can see that the $\Delta g'$ and ΔTOM deviate below 4 K but become strongly correlated above 4 K. Thus, our theory accurately predicts the general trend

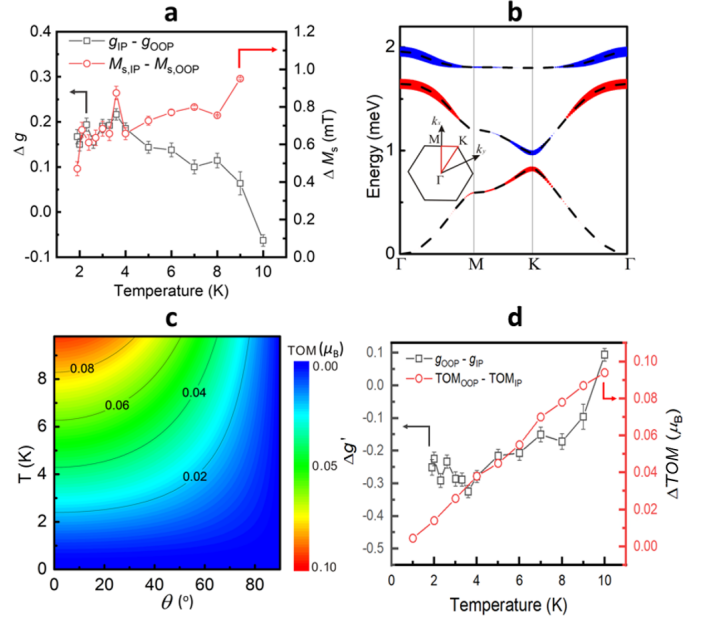


FIG. 3. Electronic Topological Orbital Moment in Cu(1,3-bdc). **a.** Temperature dependence of Δg (plotted on the left Y-axis) and ΔM_s (plotted on the right Y-axis). **b.** Flat band analysis for the magnonic bands of Cu(1,3-bdc). Red and blue colors represent the positive and negative signs of the local topological orbital moment (TOM) \mathbf{L}^{TOM} , respectively. The line thickness denotes the corresponding magnitude. The insert represents the first Brillouin Zone. The red lines connect the high symmetry points which are selected in the dispersion. **c.** TOM magnitude vs. temperature and polar angle θ . $\theta=0^\circ$ (90°) means that magnetization is along the OOP (IP) direction. The colors represent the magnitude of the integrated TOM in μ_B . Magnetic field B is assumed to be zero. **d.** $\Delta g'$ (left Y-axis) and ΔTOM (right Y-axis) as a function of temperature.

and the change in the sign of Δg observed experimentally, as shown in Fig. 3d. These facts suggest that the spin excitations can renormalize the fundamental quantum mechanical constant conventionally associated with the atomic orbital magnetism. To this end, our findings have provided experimental evidence of a new mechanism for orbital dynamics in topological magnonic systems.

Figure 4 summarizes all the orbital contributions to the magnetic moment. At low temperatures, the orbital contributions come from the motions of electrons orbiting their atomic cores for both IP and OOP cases. The black arrows in the left two illustrations represent the summation of the spin and the orbital angular momentum of the orbiting electron (red) around the nucleus (yellow). When temperature increases, the thermal fluctuations give rise to spin chirality allowed by the symmetry of the Kagome lattice in the OOP case (as shown in the right illustration). In this scenario, an electron (red) hops between a precessing noncolinear spin-triplet (yellow), generating TOM (green

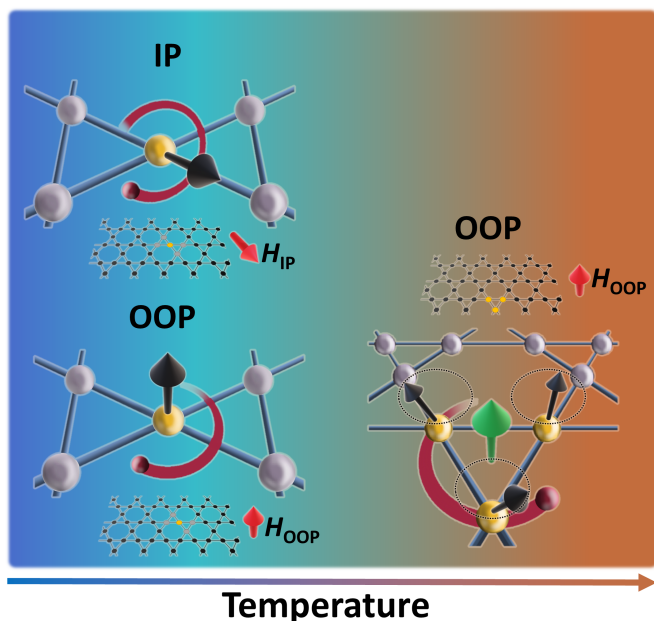


FIG. 4. Orbital Magnetic Moment. The left two illustrations show the electronic orbital moment occurring at low temperatures. The black arrows represent the overall spin and orbital moment for a field applied IP (top left) and OOP (bottom left). The right illustration shows the magnon-mediated topological orbital moment (green arrow) arising from thermally-driven scalar spin chirality.

arrow). As temperature increases, magnon scattering, such as magnon-magnon scattering and magnon-phonon scattering, causes IP and OOP orbital moment to decay. This is why the g -factor along the IP direction reduces at higher temperatures, as shown in Fig. 2f. In this regard, the increase of the g -factor along OOP with increasing temperature highlights the significance of TOM in the Cu(1,3-bdc) system.

It is helpful to identify the limiting case of the TOM effect, namely, the saturation temperature of TOM. The linear spin-wave theory we have used cannot predict the saturation temperature of TOM. Thus, we have explored the g -factor above 10 K using the FMR technique. Our results show that the FMR signals become significantly weaker and noisier above 10 K. We have estimated the g_{OOP} and g_{IP} parameters, which decay and approach $g = 2$ beyond 12 K. This indicates that TOM may saturate around 12 K.

In summary, anisotropies of Landé g -factor and saturation magnetization are observed in Cu(1,3-bdc). When $T < 4$ K, the differences of g -factor (Δg) and saturation magnetization (ΔM_s) are correlated, which indicates the contribution of orbital moment of electrons to the magnetic moment. The deviation of Δg and ΔM_s at $T > 4$ K can be explained by the spin chirality mediated by thermal fluctuations inducing sizeable electronic orbital magnetization. Our work has highlighted Cu(1,3-

bdc) as an important material platform to understand the interplay of topology, spin excitations and orbital magnetism, thereby presenting potential direction for establishing new material platforms for building novel spintronic devices. Moreover, our study has pointed a new way to probe the orbital moment in quantum magnets via the g -factor measurements. Future work that studies the chiral and topological orbital magnetism of domain walls and skyrmions[33], as well as skyrmion-topological magnon interactions in Cu(1,3-bdc) is of great interest[7].

SUPPORTING INFORMATION

The Supporting Information is available free of charge at <https://pubs.acs.org>.

Details about material preparation and characterization, ferromagnetic resonance measurement, SQUID measurement, data fittings, and theoretical calculations (PDF).

Corresponding emails: jwen11@stanford.edu, yili@anl.gov, y.mokrousov@fz-juelich.de, weizhang@oakland.edu, lipeng18@ustc.edu.cn

ACKNOWLEDGMENTS

Y.X. and W.Z. acknowledge the U.S. NSF under grant Grant Nos. ECCS-1933301 and ECCS-1941426. L.C., F.L, F.F. and Y.M. gratefully acknowledge the Jülich Supercomputing Centre and RWTH Aachen University for providing computational resources, as well as the support of Deutsche Forschungsgemeinschaft (DFG, German Research Foundation) - TRR 173 - 268565370 (project A11), TRR 288 - 422213477 (project B06). J.W. and Y.L. are supported by the U.S. Department of Energy (DOE), Office of Science, Basic Energy Sciences, Materials Sciences and Engineering Division, under contract DE-AC02-76SF00515. X.Z. acknowledges the support of the fellowship of China Postdoctoral Science Foundation No. 2021M701590. P.L. acknowledges the support of the U.S. NSF EPM Grant No. DMR-2129879, the Ralph E. Powe Junior Faculty Enhancement Award and discussions with Drs. Mingzhong Wu, Alexander Mook, Ran Cheng, and Hua Chen.

REFERENCES

-
- [1] M. Z. Hasan and C. L. Kane, "Colloquium: Topological insulators," *Rev. Mod. Phys.*, vol. 82, pp. 3045–3067, Nov

- 2010.
- [2] F. D. M. Haldane and S. Raghu, "Possible realization of directional optical waveguides in photonic crystals with broken time-reversal symmetry," *Physical review letters*, vol. 100, no. 1, p. 013904, 2008.
 - [3] S. Raghu and F. D. M. Haldane, "Analogues of quantum-hall-effect edge states in photonic crystals," *Physical Review A*, vol. 78, no. 3, p. 033834, 2008.
 - [4] F. Li, X. Huang, J. Lu, J. Ma, and Z. Liu, "Weyl points and fermi arcs in a chiral phononic crystal," *Nat. Phys.*, vol. 14, no. 1, p. 30, 2018.
 - [5] L. Zhang, J. Ren, J.-S. Wang, and B. Li, "Topological magnon insulator in insulating ferromagnet," *Phys. Rev. B*, vol. 87, p. 144101, Apr 2013.
 - [6] M. Malki and G. S. Uhrig, "Topological magnetic excitations," *EPL (Europhysics Letters)*, vol. 132, p. 20003, oct 2020.
 - [7] M. Pereiro, D. Yudin, J. Chico, C. Etz, O. Eriksson, and A. Bergman, "Topological excitations in a kagome magnet," *Nature Communications*, vol. 5, p. 4815, Sep 2014.
 - [8] M. Malki and G. S. Uhrig, "Topological magnon bands for magnonics," *Phys. Rev. B*, vol. 99, p. 174412, May 2019.
 - [9] H. Kondo, Y. Akagi, and H. Katsura, "Three-dimensional topological magnon systems," *Phys. Rev. B*, vol. 100, p. 144401, Oct 2019.
 - [10] A. Mook, S. A. Díaz, J. Klinovaja, and D. Loss, "Chiral hinge magnons in second-order topological magnon insulators," *Phys. Rev. B*, vol. 104, p. 024406, Jul 2021.
 - [11] A. A. Kovalev and V. Zyuzin, "Spin torque and nernst effects in dzyaloshinskii-moriya ferromagnets," *Phys. Rev. B*, vol. 93, no. 16, p. 161106(R), 2016.
 - [12] R. Cheng, S. Okamoto, and D. Xiao, "Spin nernst effect of magnons in collinear antiferromagnets," *Phys. Rev. Lett.*, vol. 117, no. 21, p. 217202, 2016.
 - [13] L.-c. Zhang, D. Go, J.-P. Hanke, P. M. Buhl, S. Grytsiuk, S. Blügel, F. R. Lux, and Y. Mokrousov, "Imprinting and driving electronic orbital magnetism using magnons," *Commun. Phys.*, vol. 3, no. 1, pp. 1–8, 2020.
 - [14] L. Zhang, J. Ren, J.-S. Wang, and B. Li, "Topological nature of the phonon hall effect," *Physical review letters*, vol. 105, no. 22, p. 225901, 2010.
 - [15] P. Li, W. Wu, Y. Wen, C. Zhang, J. Zhang, S. Zhang, Z. Yu, S. A. Yang, A. Manchon, and X.-x. Zhang, "Spin-momentum locking and spin-orbit torques in magnetic nano-heterojunctions composed of weyl semimetal wte2," *Nature Communications*, vol. 9, p. 3990, Sep 2018.
 - [16] R. A. Niyazov, D. N. Aristov, and V. Y. Kachorovskii, "Coherent spin transport through helical edge states of topological insulator," *npj Computational Materials*, vol. 6, p. 174, Nov 2020.
 - [17] Y. Araki, T. Misawa, and K. Nomura, "Long-range spin transport on the surface of topological dirac semimetal," *Phys. Rev. Research*, vol. 3, p. 023219, Jun 2021.
 - [18] E. A. Nytko, J. S. Helton, P. Müller, and D. G. Nocera, "A structurally perfect $s = 1/2$ metal-organic hybrid kagome antiferromagnet," *Journal of the American Chemical Society*, vol. 130, pp. 2922–2923, Mar 2008.
 - [19] R. Chisnell, J. S. Helton, D. E. Freedman, D. K. Singh, R. I. Bewley, D. G. Nocera, and Y. S. Lee, "Topological magnon bands in a kagome lattice ferromagnet," *Phys. Rev. Lett.*, vol. 115, p. 147201, Sep 2015.
 - [20] R. Chisnell, J. S. Helton, D. E. Freedman, D. K. Singh, F. Demmel, C. Stock, D. G. Nocera, and Y. S. Lee, "Magnetic transitions in the topological magnon insulator Cu(1,3-bdc) ," *Phys. Rev. B*, vol. 93, p. 214403, Jun 2016.
 - [21] D. Malz, J. Knolle, and A. Nunnenkamp, "Topological magnon amplification," *Nature Communications*, vol. 10, p. 3937, Sep 2019.
 - [22] H. Chen, T.-C. Wang, D. Xiao, G.-Y. Guo, Q. Niu, and A. H. MacDonald, "Manipulating anomalous hall antiferromagnets with magnetic fields," *Phys. Rev. B*, vol. 101, p. 104418, Mar 2020.
 - [23] R. R. Neumann, A. Mook, J. Henk, and I. Mertig, "Orbital magnetic moment of magnons," *Phys. Rev. Lett.*, vol. 125, p. 117209, Sep 2020.
 - [24] P. Li, J. Ding, S. S.-L. Zhang, J. Kally, T. Pillsbury, O. G. Heinonen, G. Rimal, C. Bi, A. DeMann, S. B. Field, W. Wang, J. Tang, J. S. Jiang, A. Hoffmann, N. Samarth, and M. Wu, "Topological hall effect in a topological insulator interfaced with a magnetic insulator," *Nano Letters*, vol. 21, pp. 84–90, Jan 2021.
 - [25] C. Oates, F. Ogrin, S. Lee, P. Riedi, G. Smith, and T. Thomson, "High field ferromagnetic resonance measurements of the anisotropy field of longitudinal recording thin-film media," *Journal of Applied Physics*, vol. 91, pp. 1417–1422, 02 2002.
 - [26] H. Chang, P. Li, W. Zhang, T. Liu, A. Hoffmann, L. Deng, and M. Wu, "Nanometer-thick yttrium iron garnet films with extremely low damping," *IEEE Magnetics Letters*, vol. 5, pp. 1–4, 2014.
 - [27] S. Khan, C. W. Zollitsch, D. M. Arroo, H. Cheng, I. Verzhbitskiy, A. Sud, Y. P. Feng, G. Eda, and H. Kurebayashi, "Spin dynamics study in layered van der waals single-crystal $\text{Cr}_2\text{Ge}_2\text{Te}_6$," *Phys. Rev. B*, vol. 100, p. 134437, Oct 2019.
 - [28] L. Alahmed, B. Nepal, J. Macy, W. Zheng, B. Casas, A. Sapkota, N. Jones, A. R. Mazza, M. Brahlek, W. Jin, M. Mahjouri-Samani, S. S.-L. Zhang, C. Mewes, L. Balicas, T. Mewes, and P. Li, "Magnetism and spin dynamics in room-temperature van der waals magnet Fe_5GeTe_2 ," *2D Materials*, vol. 8, p. 045030, sep 2021.
 - [29] S. Wimmer, S. Mankovsky, and H. Ebert, "Chirality-induced linear response properties in non-coplanar Mn_3Ge ," *Phys. Rev. B*, vol. 103, no. 2, p. 024437, 2021.
 - [30] S. Grytsiuk, J.-P. Hanke, M. Hoffmann, J. Bouaziz, O. Gomonay, G. Bihlmayer, S. Lounis, Y. Mokrousov, and S. Blügel, "Topological-chiral magnetic interactions driven by emergent orbital magnetism," *Nat. Commun.*, vol. 11, no. 1, pp. 1–7, 2020.
 - [31] J.-P. Hanke, F. Freimuth, S. Blügel, and Y. Mokrousov, "Prototypical topological orbital ferromagnet $\gamma\text{-FeMn}$," *Sci. Rep.*, vol. 7, p. 41078, 2017.
 - [32] J.-P. Hanke, F. Freimuth, A. K. Nandy, H. Zhang, S. Blügel, and Y. Mokrousov, "Role of berry phase theory for describing orbital magnetism: From magnetic heterostructures to topological orbital ferromagnets," *Phys. Rev. B*, vol. 94, no. 12, p. 121114(R), 2016.
 - [33] F. R. Lux, F. Freimuth, S. Blügel, and Y. Mokrousov, "Engineering chiral and topological orbital magnetism of domain walls and skyrmions," *Commun. Phys.*, vol. 1, no. 1, p. 60, 2018.